

# DIFFERENTIAL EXPANSION OF SPACE AND THE HUBBLE FLOW ANISOTROPY

KRZYSZTOF BOLEJKO

Sydney Institute for Astronomy, School of Physics, A28, University of Sydney, Camperdown NSW 2006, Australia

M. AHSAN NAZER, AND DAVID L. WILTSHIRE

Department of Physics & Astronomy, University of Canterbury, Private Bag 4800, Christchurch 8140, New Zealand

*Draft version June 1, 2019*

## ABSTRACT

The Universe on scales  $10\text{--}100 h^{-1}\text{Mpc}$  is dominated by a cosmic web of voids, filaments, sheets and knots of galaxy clusters. These structures participate differently in the global expansion of the Universe: from non-expanding clusters to the above average expansion rate of voids. In this paper we characterize Hubble expansion anisotropies in the COMPOSITE sample of 4534 galaxies and clusters. We concentrate on the dipole and quadrupole in the rest frame of the Local Group. These both have statistically significant amplitudes. These anisotropies, and their redshift dependence, cannot be explained solely by a boost of the Local Group in the Friedmann-Lemaître-Robertson-Walker (FLRW) model which expands isotropically in the rest frame of the cosmic microwave background (CMB) radiation. We simulate the local expansion of the Universe with inhomogeneous Szekeres models, which match the standard FLRW model on  $\gtrsim 100 h^{-1}\text{Mpc}$  scales but exhibit nonkinematic differential expansion on small scales. We restrict models to be consistent with observed CMB temperature anisotropies, while simultaneously fitting the redshift variation of the Hubble expansion dipole. We include features to account for both the Local Void and the “Great Attractor”. While this naturally accounts for the Hubble expansion and CMB dipoles, the simulated quadrupoles are smaller than observed. Further refinement to incorporate additional structures may improve this. This would enable a test of the hypothesis that some large angle CMB anomalies result from failing to treat the differential expansion of space; a natural feature of Einstein’s equations not included in the current standard model of cosmology.

*Subject headings:* cosmology: theory — cosmology: observations — large-scale structure of universe — cosmology: cosmic background radiation

## 1. INTRODUCTION

In the standard cosmology deviations from a uniform expansion are most commonly treated as peculiar velocities relative to a linear Hubble law

$$v_{\text{pec}} = cz - H_0 r \quad (1)$$

where  $z$  is the redshift,  $c$  the speed of light,  $r$  an appropriate distance measure, and  $H_0 \equiv H(t_0) = 100 h \text{ km s}^{-1} \text{ Mpc}^{-1}$  is the Hubble constant,  $h$  being a dimensionless number. Such a theoretical framework is a natural description if the assumption of homogeneity and isotropy holds at all scales, so that all cosmologically relevant motions can be understood in terms of the background expansion of one single Friedmann-Lemaître-Robertson-Walker (FLRW) geometry, with a Hubble parameter,  $H(t)$ , given by the Friedmann equation, plus local boosts which can be treated by eq. (1) for suitably small values of the distance,<sup>1</sup>  $r$ .

However, the universe is only spatially homogeneous in some statistical sense when one averages on scales  $\gtrsim 100 h^{-1}\text{Mpc}$ . Below this scale the universe exhibits strong inhomogeneities, characterized in particular by a population of voids (Pan et al. 2012) with density con-

trasts close to the minimum possible  $\delta\rho/\rho = -1$ . In fact, voids of a typical diameter  $30 h^{-1}\text{Mpc}$  and density contrast  $\delta\rho/\rho \lesssim -0.95$  form some 40% of the volume of the late epoch universe (Hoyle & Vogeley 2002, 2004), and given the presence of numerous smaller minivoids (Tikhonov & Karachentsev 2006), the present epoch universe is void dominated – the precise volume fraction depending on exactly how voids are defined. Galaxies and clusters of galaxies — the cosmological particles whose motions are investigated via (1) — are not themselves randomly distributed but are strung in filaments that threads the voids, and sheets that surround them, forming a complex cosmic web (Forero-Romero et al. 2009; Bilicki et al. 2014; Einasto et al. 2014).

At the present epoch, the FLRW geometry can only be observationally justified on the  $\gtrsim 100 h^{-1}\text{Mpc}$  scales on which some notion of homogeneity is observed statistically. Just how large this scale is, is debated (Hogg et al. 2005; Sylos Labini et al. 2009; Scrimgeour et al. 2012; Clowes et al. 2013; Roukema et al. 2015). However, based on the fractal dimension of the 2-point galaxy correlation function making a gradual transition to the homogeneous limit  $D_2 \rightarrow 3$  in three spatial dimensions, a scale of statistical homogeneity in the range  $70 \lesssim r_{\text{ssh}} \lesssim 120 h^{-1}\text{Mpc}$  seems to be observed (Scrimgeour et al. 2012).

Despite the fact that the FLRW geometry can only be

<sup>1</sup> Even within FLRW models, for large values of  $r$  one has to take into account that  $H(t)$  varies with time, and that the redshift is not additive but rather a multiplicative quantity, so a simple addition as in (1) does not apply:  $1 + z_{1+2} = (1 + z_1)(1 + z_2) \neq 1 + z_1 + z_2$ .

observationally justified on  $\gtrsim 100 h^{-1}\text{Mpc}$  scales, by tradition it is conventionally assumed that such a geometry is still applicable at all scales on which space is expanding below  $r_{\text{ssh}} \sim 100 h^{-1}\text{Mpc}$ , that is, until one gets to the very small scales of bound clusters of galaxies. However, this assumption is not justified by the principles of general relativity. In general, solutions of Einstein's equations space does not expand rigidly to maintain constant spatial curvature as it does in the FLRW geometry. General inhomogeneous cosmological models, such as the Lemaitre–Tolman (LT) (Lemaitre 1933; Tolman 1934; Bondi 1947) and Szekeres (1975a) models, exhibit differential expansion of space. The Hubble parameter becomes a function of space as well as time, and any relation (1) can no longer have the physical sense of defining a peculiar velocity field with respect to a single expansion rate.

In this paper we will present the results of numerical investigations that quantify the nonlinearity associated with differential expansion of space in Szekeres models chosen to match key features of both the Cosmic Microwave Background (CMB) anisotropies, and also the Hubble expansion on  $\lesssim 100 h^{-1}\text{Mpc}$  scales. The crucial feature in these simulations is that the dipole is induced by local inhomogeneities and cannot be directly attributed to a  $635 \text{ km s}^{-1}$  local boost of the Local Group (LG).

Despite its naturalness in general relativity, the hypothesis of a nonkinematic origin for a fraction of the CMB dipole goes against the consensus of what has been assumed in observational cosmology (Stewart & Sciamia 1967; Peebles & Wilkinson 1968) ever since the first bounds were placed on the anisotropy of the CMB in the 1960s (Partridge & Wilkinson 1967). By now it is standard practice to automatically transform redshift data to the CMB rest frame before performing cosmological analyses.

As the accuracy of measurements improves, we should expect to detect observational consequences from treating a nonkinematic dipole purely as a local boost, even if the full general relativistic case may give results which are very close to a Newtonian treatment (Alnes & Amarzguioui 2006). In fact, over the past decade several large angle anomalies have been observed in the CMB anisotropy spectrum (Tegmark et al. 2003; Eriksen et al. 2004; de Oliveira-Costa et al. 2004; Schwarz et al. 2004; Land & Magueijo 2005; Copi et al. 2006; Eriksen et al. 2007; Hoftuft et al. 2009; Kim & Naselsky 2010) and the statistical significance of some of these problems has increased with the release of Planck satellite data (Ade et al. 2014b). Since the problem we study here potentially has a direct relationship to resolving such anomalies, it may be highly significant for observational cosmology.

There have been a number of previous studies which have used the LT model to model the effects of anisotropic expansion (Arnau et al. 1993, 1994; Humphreys et al. 1997; Tomita 2000; Alnes & Amarzguioui 2006; Bolejko & Hellaby 2008; Bolejko et al. 2013; Bacon et al. 2014), including its effects on the CMB. However, these have typically considered the effects of voids at large distances from our loca-

tion, or the effects of voids much larger than the small scale inhomogeneities we will consider. Where attempts have been made to model nearby structures such as the Great Attractor and Shapley Concentration using the LT model (Tomita 2000; Bolejko & Hellaby 2008), these investigations have simply sought to obtain effective peculiar velocities commensurate with those determined in the standard analysis of bulk flows.

To our knowledge this paper contains the first ever study which seeks to use exact solutions of Einstein's equations to model nonlinear structures on scales comparable to those observed, constrained directly by both ray-tracing of the CMB and by the Hubble expansion field from actual surveys. While the Szekeres model has been employed for a number of cosmological problems (Bolejko 2009; Bolejko & C  lerier 2010; Nwankwo et al. 2011; Ishak & Peel 2011; Bolejko & Sussman 2011; Buckley & Schlegel 2013; Sussman & Gaspar 2015a,b), we believe that this is also the first time that it has been used for ray-tracing simulations of local structures. We will see that although we are not able to match all features of the nonlinear Hubble expansion below the statistical homogeneity scale, with the Szekeres model we can nonetheless match more features of the actual data than with other models, including the standard FLRW cosmology with a local boost of the Local Group of galaxies. This paper provides a proof-of-principle demonstration that we hope will encourage even more sophisticated investigations of relativistic effects beyond the standard model.

## 2. THE NONLINEAR REGIME

Let us begin by making clear the distinction between the nonlinear effects of interest in this paper, and other common uses of such terminology.

### 2.1. Large scale homogeneous isotropic radial nonlinearity

Independently of the energy momentum tensor, the luminosity distance relation of any FLRW cosmology can be Taylor expanded at low redshifts to give

$$d_L(z) = \frac{c}{H_0} \left\{ z + \frac{1}{2} [1 - q_0] z^2 - \frac{1}{6} \left[ 1 - q_0 - 3q_0^2 + j_0 + \frac{kc^2}{H_0^2 a_0^2} \right] z^3 + O(z^4) \right\} \quad (2)$$

where  $d_L$  is the luminosity distance to the observed galaxy,  $q_0$  the deceleration parameter,  $j_0$  the jerk parameter,  $a_0 = a(t_0)$  the present cosmic scale factor, and  $k = -1, 0, 1$  the spatial curvature. The  $O(z^2)$  and higher order terms represent nonlinear corrections to the linear Hubble law.

Even if the Universe is not described by a FLRW model, but by some alternative in which a notion of statistical homogeneity applies, then we can still expect a cosmic expansion law with a Taylor series in  $z$  similar to (2). This is the case for the timescape cosmology (Wiltshire 2007a,b, 2009; Duley et al. 2010), for example. However, in such cases the higher order coefficients

will not have the form given in (2). In particular, generically averages of inhomogeneous models do not expand in such a way as to maintain a rigid constant spatial curvature,  $k$ .

## 2.2. Small scale nonlinearities

Even if the FLRW model is a good fit on large scales, the Taylor expansion (2) is only *a priori* justified on scales  $d_L \gtrsim r_{\text{ssh}}$  on which a notion of statistical homogeneity applies. Small scale differences will lead to a complex nonlinear regime, producing redshift–space distortions that affect all cosmological observations. For more distant objects the redshift–space distortions at the source will lead to small uncertainties as a fraction of the overall distance. However, in our own vicinity on scales  $d_L \lesssim r_{\text{ssh}}$  these effects can be large.

There is no uniform approach to the placement of the boundary between the linear and nonlinear regimes in our vicinity. On one hand, in determining the Hubble constant, Riess et al. (2011) exclude data  $z < 0.024$ , or  $d_L \lesssim 72 h^{-1}\text{Mpc}$ . On the other hand, cosmological parameter fits based on Type Ia supernovae often include significant amounts of data with  $0.015 \leq z \leq 0.023$  (Kowalski et al. 2008; Amanullah et al. 2010), and sometimes extend the range down to  $z \geq 0.01$  (Hicken et al. 2009). Our own analysis is based on the assumption that we can expect a nonlinear regime to extend to distances  $d_L \sim 70 h^{-1}\text{Mpc}$  from our location, as is consistent with the scale of the observed emergence of homogeneity in large galaxy surveys (Scrimgeour et al. 2012).

In the standard cosmology small scale inhomogeneities in the nonlinear regime are investigated with large  $N$ -body numerical simulations using Newtonian gravity in a uniformly expanding box, with an expansion rate fit to a Lambda Cold Dark Matter ( $\Lambda\text{CDM}$ ) model. By construction, such models do not allow the possibility of a nonkinematic differential expansion.

In order to construct any numerical simulation some model is required. In this paper, we will perform simulations with the Szekeres model, which does allow for nonkinematic differential expansion. However, we will first discuss the recent model-independent investigation of the Hubble expansion in the nonlinear regime, which motivated the present study.

## 2.3. Model independent characterization of small scale nonlinear expansion

In recent work (Wiltshire et al. 2013; McKay & Wiltshire 2015) the problem of characterizing the Hubble expansion below  $r_{\text{ssh}}$  was approached with no prior assumptions about the homogeneity of the spatial geometry. In particular, given a large data set with good sky coverage, one can simply determine the best fit average linear Hubble law in radial shells, even in the regime in which the expansion is nonlinear, a technique first used by Li & Schwarz (2008). Another alternative is to take angular averages, for example, by employing a Gaussian window averaging method pioneered by McClure & Dyer (2007).

Wiltshire et al. (2013) applied these techniques to the COMPOSITE sample of 4,534 galaxies and clusters compiled from earlier surveys by Watkins et al. (2009); Feldman et al. (2010). A startling result was found —

when the best fit spherically averaged Hubble parameter in inner shells was compared to the asymptotic value on  $r > 156 h^{-1}\text{Mpc}$  scales, it was found that the Hubble expansion was more uniform in the rest frame of the Local Group (LG) of galaxies than in the standard CMB rest frame, with very strong Bayesian evidence. There is no reason why this should be true in the standard cosmology. The cosmic rest frame should naturally coincide with the frame in which the Hubble expansion is most uniform, with minimum statistical variations.

It was argued by Wiltshire et al. (2013) that an arbitrary boost,  $v$ , of the central observer from a rest frame in which the Hubble parameter,  $H$ , is close to uniform will display a systematic offset of the value  $H'$  determined by least squares regression in spherical shells in the boosted frame. In particular, when minimizing the sum  $\chi_s^2 = \sum_i [\sigma_i^{-1}(r_i - cz'_i/H')]^2$  with respect to  $H'$ , where  $r_i$  and  $\sigma_i$  are individual distances and their uncertainties, under a boost of the central observer the original redshifts transform as  $cz_i \rightarrow cz'_i = cz_i + v \cos \phi_i$  for small  $v$ , where  $\phi_i$  is the angle between each data point and the boost direction. Provided the number density of objects in a distance catalogue is balanced on opposite sides of the sky, then terms linear in the boost cancel from opposite sides of the sky in a spherical average, leaving a term proportional to  $v^2$ . The offset is found to give approximately

$$H' - H \simeq \frac{v^2}{2\bar{H}_0 \langle r_i^2 \rangle}, \quad (3)$$

in successive radial shells, where  $\bar{H}_0$  is the asymptotic Hubble constant in the range where expansion is linear. McKay & Wiltshire (2015) found that such a signature is indeed observed between the CMB and LG rest frames in both the COMPOSITE sample (Watkins et al. 2009; Feldman et al. 2010), and in the larger *Cosmicflows-II* (CF2) sample (Tully et al. 2013).

It was also found by Wiltshire et al. (2013) that the largest residual monopole variation in the Hubble expansion in the LG rest frame occurs in a range  $40 h^{-1} - 60 h^{-1}\text{Mpc}$ , whereas the monopole variation in the CMB frame is less than in the LG frame in this range only. Over the same distance range  $H' - H$  is found to deviate from the relation (3) in both the COMPOSITE and CF2 catalogues<sup>2</sup>. Angular averages reveal a dipole structure in the Hubble expansion, whose amplitude changes markedly over the range  $32 h^{-1} - 62 h^{-1}\text{Mpc}$ , in different ways in the two rest frames. The conclusion from various analyses (Wiltshire et al. 2013) is that the boost from the LG frame to the CMB frame appears to be compensating for the effect on cosmic expansion of inhomogeneous structures within this distance range. A boost to the CMB frame has the effect of almost cancelling the monopole and dipole variations; but not perfectly. Whereas the amplitude of the dipole expansion varia-

<sup>2</sup> The reported CF2 distances include untreated distribution Malmquist biases (Tully et al. 2013) which lead to an additional spurious monopole (Hoffman et al. 2015; McKay & Wiltshire 2015) when spherical averages are taken. Despite this bias the signature (3) is still apparent in the CF2 catalogue in the *difference*  $H' - H$ , but with a somewhat broader distance range,  $30 h^{-1} \lesssim r \lesssim 67 h^{-1}\text{Mpc}$ , over which (3) does not apply, consistent with there being additional systematic uncertainties in individual distances (McKay & Wiltshire 2015).

tion declines to levels statistically consistent with zero for  $r \gtrsim 65 h^{-1}\text{Mpc}$  in the LG frame, in the CMB frame the dipole amplitude drops to a minimum value close to zero at  $r \sim 44 h^{-1}\text{Mpc}$ , but subsequently increases (Wiltshire et al. 2013).

Finally, using Gaussian window averages, a skymap of angular Hubble expansion variation on  $r > 15 h^{-1}\text{Mpc}$  scales was determined for the COMPOSITE sample and its correlation coefficient,  $\mathcal{C}$ , with the residual CMB dipole in the LG frame was computed. It was found that  $\mathcal{C} = -0.92$  for an angular smoothing scale  $\sigma_\theta = 25^\circ$ , which was almost unchanged as the smoothing scale was varied in the range  $15^\circ < \sigma_\theta < 40^\circ$ .

The combination of the above results led to the hypothesis of Wiltshire et al. (2013) that a significant component of the observed CMB dipole, which is conventionally attributed to a local motion of the Local Group of galaxies by an amount  $v_p = 635 \pm 38 \text{ km s}^{-1}$  in a direction  $(\ell, b) = (276.4^\circ, 29.3^\circ) \pm 3.2^\circ$ , is nonkinematic in origin. It should be attributed to a differential expansion of space, due to foreground inhomogeneities on  $\lesssim 65 h^{-1}\text{Mpc}$  which result in a 0.5% anisotropy in the distance–redshift relation below these scales.

From the point of view of general relativity, such a hypothesis is not surprising — it is simply a property of general inhomogeneous cosmological models. Indeed, using a simple Newtonian approximation (Alnes & Amarzguioui 2006) for LT models (Lemaître 1933; Tolman 1934; Bondi 1947), numerical estimates of the size of the effect were made by Wiltshire et al. (2013). These were indeed consistent observationally both in terms of the the magnitude of the CMB temperature dipole and quadrupole, and the scale of the void relative to that of the actual structures observed in the nearby universe (Erdoğdu et al. 2006).

### 3. THE OBSERVATIONAL DATA

#### 3.1. The anisotropy of the Hubble expansion

At low redshifts the Hubble constant for a spatially flat FLRW universe can be calculated by rearranging the terms of (2) to obtain

$$H_0 = \frac{c}{d_L} \left[ z + \frac{1}{2}(1 - q_0)z^2 - \frac{1}{6}(1 - q_0 - 3q_0^2 + j_0)z^3 \right]. \quad (4)$$

Given a large set of data with independently measured values of  $z$  and  $d_L$  one could determine  $H_0$ ,  $q_0$  and  $j_0$  for any spatially homogeneous isotropic cosmology using the above formula. In practice, with current data one is only able to independently determine  $H_0$  at low redshifts, and when terms beyond the linear Hubble law are used in (4) then fixed values of  $q_0$  and  $j_0$  must be assumed from other observations. For example, the Riess et al. (2011) estimate assumes values  $q_0 = -0.55$  and  $j_0 = 1$  consistent with a spatially flat  $\Lambda\text{CDM}$  model with  $\Omega_m = 0.3$ .

Wiltshire et al. (2013) and McKay & Wiltshire (2015) analysed the COMPOSITE sample using only the term linear in  $z$  as they were interested in a model-independent analysis of the variation of the Hubble expansion. In the present paper, we are interested in testing a cosmological model which has the properties of a Planck satellite normalized spatially flat FLRW model

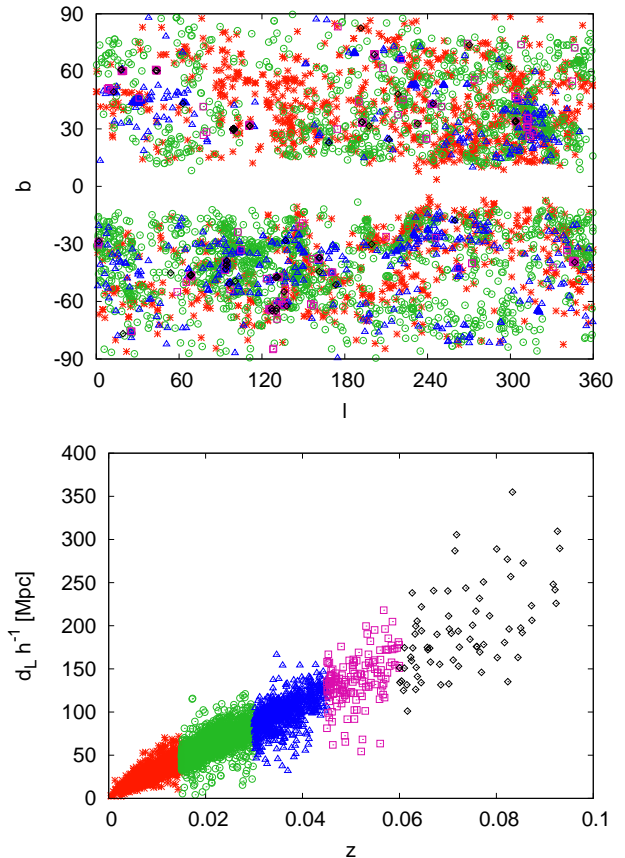


**Figure 1.** The COMPOSITE sample. *Upper Panel:* angular distribution of galaxies in the Galactic coordinates  $\ell$  and  $b$ ; *Lower Panel:* distance vs LG frame redshift;  $z \leq 0.015$  red stars,  $0.015 < z \leq 0.03$  green circles,  $0.03 < z \leq 0.045$  blue triangle,  $0.045 < z \leq 0.06$  magenta square,  $z > 0.06$  black diamonds.

at distances  $d_L \gg 100 h^{-1}\text{Mpc}$  but with nonlinear structures on smaller scales, modelled by exact solutions of Einstein’s equations. We will therefore firstly reanalyse the COMPOSITE sample using (4) with  $q_0 = -0.5275$  and  $j_0 = 1$ , consistent with the best fit value  $\Omega_m = 0.315$  of Ade et al. (2014a).

As seen from Fig. 1, except for the Zone of Avoidance region obscured by our Galaxy ( $|b| \lesssim 15^\circ$ ), the COMPOSITE sample has good angular coverage<sup>3</sup>, and thus can be used to evaluate large angle anisotropies of the Hubble expansion (dipole and quadrupole). However, the COMPOSITE sample has large uncertainties associated with the distance measure.

From the point of view of propagation of uncertainty, it is better to work with the formula (2) with  $d_L$  as the independent variable in the numerator. To infer  $H_0$  from the data we therefore minimize the following sum

$$\chi^2 = \sum_i \left( \frac{d_i - c\zeta_i/H_0}{\Delta d_i} \right)^2, \quad (5)$$

<sup>3</sup> This statement remains true when the data is broken into concentric radial shells in distance, as is seen in Fig. 2 of Wiltshire et al. (2013), where only the innermost of 11 radial shells (with  $d_L < 18.75 h^{-1}\text{Mpc}$ ) was found to have insufficient sky coverage when performing statistical checks.

where

$$\zeta_i = \left[ z_i + \frac{1}{2}(1 - q_0)z_i^2 - \frac{1}{6}(1 - q_0 - 3q_0^2 + j_0)z_i^3 \right], \quad (6)$$

$d_i$  and  $z_i$  are respectively the luminosity distance and redshift of each object in the COMPOSITE sample, and  $\Delta d_i$  is the distance uncertainty. The above is equivalent to calculating the Hubble constant as a weighted average,

$$H_0 = \frac{\sum_i H_i w_{d,i}}{\sum_i w_{d,i}}, \quad (7)$$

where

$$H_i = c\zeta_i/d_i \quad (8)$$

and

$$w_{d,i} = c\zeta_i d_i / (\Delta d_i)^2. \quad (9)$$

Wiltshire et al. (2013) evaluated (7) for spherical averages in independent radial shells, for the case of a linear Hubble law with  $\zeta_i = z_i$ , and separately considered angular averages using a Gaussian window function smoothing in solid angle.

Here we will apply Gaussian window function smoothing jointly in both solid angle and redshift, to obtain the following formula for the average local Hubble constant centred at galactic coordinates  $(\ell, b)$  and redshift,  $z$ ,

$$H_0(\ell, b, z) = \frac{\sum_i H_i w_{d,i} w_{z,i} w_{\theta,i}}{\sum_i w_{d,i} w_{z,i} w_{\theta,i}}, \quad (10)$$

where  $H_i$  and  $w_{d,i}$  are given by (8) and (9) respectively, while

$$w_{z,i} = \frac{1}{\sqrt{2\pi}\sigma_z} \exp \left[ -\frac{1}{2} \left( \frac{z - z_i}{\sigma_z} \right)^2 \right], \quad (11)$$

$$w_{\theta,i} = \frac{1}{\sqrt{2\pi}\sigma_\theta} \exp \left[ -\frac{1}{2} \left( \frac{\theta_i}{\sigma_\theta} \right)^2 \right], \quad (12)$$

$\sigma_z = 0.01$ ,  $\sigma_\theta = 25^\circ$ , and  $\theta_i$  is the angle between the direction of each source  $(\ell_i, b_i)$  and the direction of any given point on the sky,  $(\ell, b)$ :

$$\cos \theta_i = \cos b \cos b_i \cos(\ell - \ell_i) + \sin b \sin b_i.$$

For  $w_{z,i} = 1$  — i.e., with no redshift smoothing — equations (10) and (12) reduce to equations (B5) and (B9) derived in Appendix B of Wiltshire et al. (2013) using a procedure based on minimizing the scatter in  $H^{-1}$ . We adopt their optimal value  $\sigma_\theta = 25^\circ$  for the smoothing scale in angular averages, but our smoothing scale in redshift,  $\sigma_z = 0.01$ , is larger than the effective width of the shells used by Wiltshire et al. (2013) for their purely spherical averages. When simultaneously taking an average in both redshift and solid angle then a larger  $\sigma_z$  is demanded to obtain statistically reliable results given the distribution of data in the COMPOSITE sample.

Using (10) we calculate the regional contributions to our locally measured Hubble constant on an angular and redshift grid. For each redshift value on the grid, we construct the angular maps of the Hubble expansion and express the Hubble flow in terms of its fluctuations

$$\frac{\Delta H_0}{\langle H_0 \rangle} = \frac{H_0(\ell, b, z) - \langle H_0 \rangle}{\langle H_0 \rangle}, \quad (13)$$

where

$$\langle H_0 \rangle = \frac{\int d\Omega H_0(\ell, b, z)}{4\pi}, \quad (14)$$

is the spherically averaged value of (10).

For each redshift, the fluctuations (13) are then analysed using the spherical harmonic decomposition

$$\frac{\Delta H_0}{H_0} = \sum_{l,m} a_{lm} Y_{lm}, \quad (15)$$

which allows us to evaluate the angular power spectrum:

$$C_l = \frac{1}{2l+1} \sum_m |a_{lm}|^2. \quad (16)$$

The power spectrum is calculated using the HEALPix package (Górski et al. 2005). The dipole  $C_1$  and quadrupole  $C_2$  of our regional Hubble expansion using the above procedure are presented as a function of redshift in Fig. 2.

### 3.2. Completeness and robustness

As seen from Fig. 1, and in more detail in Fig. 2 of Wiltshire et al. (2013), there is good angular coverage in the COMPOSITE data. Potential systematic uncertainties from anisotropies generated by insufficient sky cover were investigated in detail by Wiltshire et al. (2013), who performed 12 million random reshuffles of the data in independent spherical shells, with the conclusion that for a binning scale  $\Delta d = 12.5 h^{-1} \text{Mpc}$  (or  $\Delta z \simeq 0.004$ ) results concerning the dipole anisotropy were robust on scales  $0.002 < z < 0.04$ , with up to 99.999% confidence in some ranges.

In our case, we are also investigating the quadrupole anisotropy and adopt the larger redshift smoothing scale  $\Delta z = 0.01$ . However, there is still a possibility that the inferred anisotropy could result from some biases in the data. To minimize any systematic bias and to confirm that the measured anisotropy is not spurious, we performed the following checks:

- We used the fluctuations (15) rather than the spherical average (7). In the hypothetical case of an exactly homogeneous and isotropic universe (and perfect measurements)  $\Delta H_0 = 0$ , so even if we have all the data only in one part of the sky and the rest of the sky without any measurement we should not detect any anisotropy.
- We shuffled the data. We tested the robustness of the results on the dipole and quadrupole anisotropies by analyzing the reshuffled data — for each pair of  $z$  and  $d_L$  we randomly reshuffled the angular position. We generated 100,000 reshuffled COMPOSITE catalogues and calculated the dipole and quadrupole of the Hubble expansion. If the measured signal were comparable with the signal obtained from reshuffled samples that would indicate that the original result is spurious. That was not the case, however.
- We used half of the data. An alternative test of robustness was performed by taking half of the COMPOSITE sample to calculate the dipole

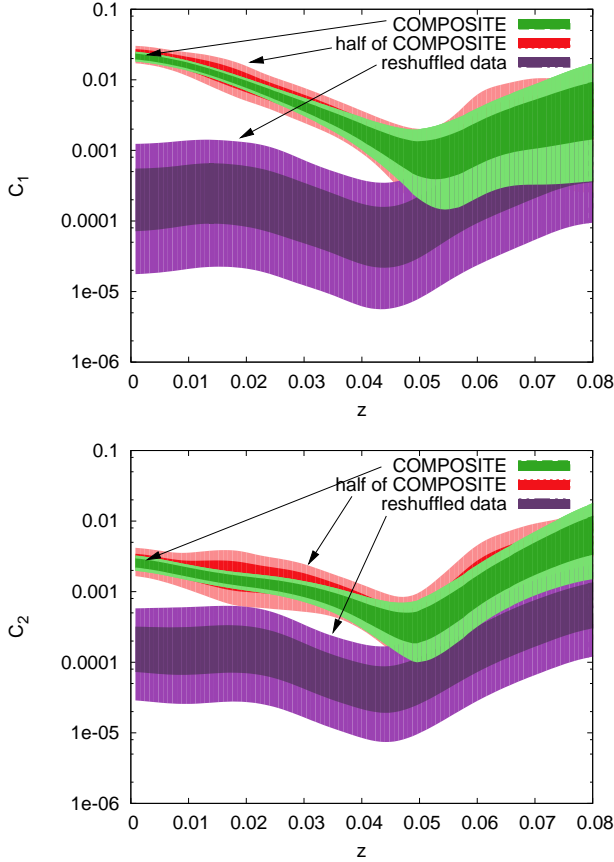


**Figure 2.** The anisotropy of the Hubble expansion in the LG frame: dipole (*Upper Panel*) and quadrupole (*Lower Panel*). The green bands show the 65% and 95% confidence intervals for the COMPOSITE sample. The red bands show the 65% and 95% confidence intervals obtained using 100,000 random halves of the COMPOSITE sample. The purple bands show the 65% and 95% confidence intervals obtained using 100,000 random reshuffles of the COMPOSITE sample.

and quadrupole anisotropies of the Hubble expansion. This was done for 100,000 randomly selected halves of the original COMPOSITE catalogue. If the measured signal was not consistent with the anisotropy obtained from half of the sample that would indicate that the original result is spurious. Again, this was not the case.

The results of the above analyses are combined in Fig. 2. As seen our analysis passes these tests at the  $2\sigma$  level for  $z \lesssim 0.045$ . This is consistent with the more exhaustive tests of Wiltshire et al. (2013), which showed that the dipole is not a systematic effect, to very high confidence.

### 3.3. Kinematic interpretation of anisotropies

The results presented in Fig. 2 indicate the presence of anisotropy in the Hubble expansion up to  $z \sim 0.045$ , as determined from the COMPOSITE sample redshifts transformed to the LG rest frame. The anisotropy is largest for small redshifts  $z \sim 0.02$ , with the amplitude of the dipole dropping one order of magnitude from  $z = 0.02$  to  $z = 0.045$ , from which point the dipole amplitude is consistent with that of the randomly reshuffled data at  $2\sigma$ .

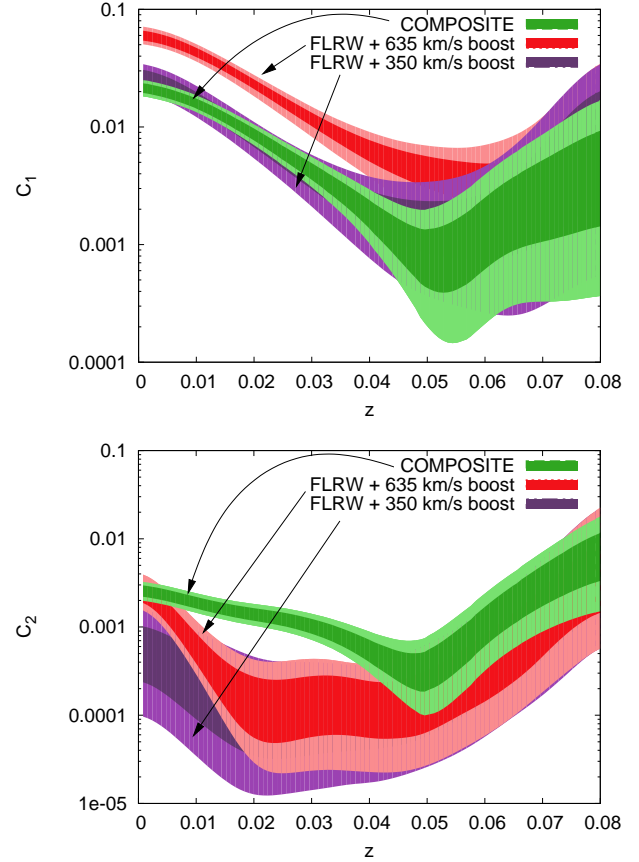


**Figure 3.** The anisotropy of the Hubble expansion: dipole (*Upper Panel*) and quadrupole (*Lower Panel*). The green bands show the 65% and 95% confidence intervals for the COMPOSITE sample. The red bands show the 65% and 95% confidence intervals obtained using mock COMPOSITE catalogues based on FLRW redshifts corrected by the local boost of 635 km/s.

According to the conventional explanation the anisotropy of the Hubble expansion observed in Fig. 2 should have a kinematic origin, due to a boost of

$$v_o = 635 \pm 38 \text{ km s}^{-1} \quad (17)$$

in the direction

$$(\ell_o, b_o) = (276.4^\circ, 29.3^\circ) \pm 3.2^\circ, \quad (18)$$

from the LG to CMB rest frame. This hypothesis can be directly tested by assuming a spatially homogeneous universe in the CMB frame, generating mock COMPOSITE samples in that frame, adjusting the redshift by performing a local boost to the LG frame, and then analysing the mock data in the manner of Fig. 2. Specifically,

1. We take the COMPOSITE sample. For each galaxy we have its angular position  $(\ell_i, b_i)$ , luminosity distance  $d_i$ , uncertainty in distance  $\Delta d_i$  and redshift  $z_i$ . For each of these directions  $(\ell_i, b_i)$  we use the  $\Lambda$ CDM model to find the redshift ( $z_{\text{FLRW}}$ ) at which  $d_L = d_i$ , by solving

$$d_L = (1+z) \frac{c}{H_0} \int_0^{z_{\text{FLRW}}} dz \frac{1}{\sqrt{\Omega_m(1+z)^3 + 1 - \Omega_m}},$$

with  $\Omega_m = 0.315$ , corresponding to the best fit



parameters from the Planck satellite (Ade et al. 2014a). (We also take the Planck satellite normalized  $H_0 = 67.3 \text{ km s}^{-1} \text{ Mpc}^{-1}$ . However, since we normalize all distances to  $h^{-1} \text{ Mpc}$ , this is inconsequential.)

2. We adjust the redshift for the local boost

$$1 + z_{\text{FLRW-B}} = \gamma(1 - \beta_o \cos \theta)(1 + z_{\text{FLRW}}) \\ \simeq (1 - \beta_o \cos \theta)(1 + z_{\text{FLRW}}), \quad (19)$$

where  $\beta_o = v_o/c = (2.1 \pm 0.1) \times 10^{-3}$  by (17), while

$$\cos \theta = \cos b_o \cos b_i \cos(\ell_o - \ell_i) + \sin b_o \sin b_i,$$

$\ell_o$  and  $b_o$  being given by (18), and we have set  $\gamma = (1 - \beta_o^2)^{-1/2} \simeq 1$ , ignoring terms of  $O(\beta_o^2)$ .

3. We construct the mock COMPOSITE catalogue in the LG frame, by replacing  $z_i$  with  $z_{\text{FLRW-B}}$ , (i.e., the redshift obtained in the FLRW model adjusted for the motion of the LG).
4. We construct 100,000 mock catalogues, using the actual distance uncertainties from the COMPOSITE sample and also taking into account the uncertainties in (17), (18).
5. For each of these mocks catalogues we calculate the Hubble expansion and its anisotropy as outlined in Sec. 3.1.

The results are presented in Fig. 3. As seen the anisotropy produced by a FLRW model with local boost is characterized by a dipole three times larger than is observed in the COMPOSITE data at low redshift, and differs by more than  $2\sigma$  for all redshifts  $z < 0.04$ . On the other hand the quadrupole generated by the FLRW model with local boost is comparable to that of the COMPOSITE sample as  $z \rightarrow 0$ , but becomes smaller than that of the COMPOSITE sample for  $z \gtrsim 0.01$ , being consistent with that of the randomly reshuffled data in Fig. 2. Thus for  $z > 0.01$  the local boost of 635 km/s cannot account for the amplitude of the observed quadrupole in the COMPOSITE sample.

We note that the linear  $\cos \theta$  dependence in (19) gives rise to a pure dipole anisotropy at fixed values of  $z_{\text{FLRW}}$  and  $d_L$  in a linear Hubble relation. However, once (19) is substituted in the Taylor series (6), a quadrupole and higher order multipoles are also generated at fixed redshift. The amplitude of the boosted quadrupole in Fig. 3 is larger than would be produced with perfect data, the ratio of the boost quadrupole and dipole contributions to (15) generated by (6) and (19) being proportional to  $\beta_o^2 \sim 4 \times 10^{-6}$ . The relatively large value of the ratio  $C_2/C_1 \sim 0.05$  reflects the combination of the effect of angular smoothing in the Gaussian window average (10)–(12) with the actual distance uncertainties assigned to the mock data, leading to  $C_2 \sim 0.004$  at low redshift for the randomly reshuffled COMPOSITE data in Fig. 2.

We have investigated by how much the magnitude of the local boost on the axis of the CMB and LG frames must be reduced in order to match the Hubble expansion dipole of the COMPOSITE sample. We find that a 350 km/s boost would match the Hubble expansion

dipole, giving results which are also shown in Fig. 3. The quadrupole of the COMPOSITE sample is not matched, however. For a 350 km/s boost the quadrupole is consistent with the residual level of the randomly reshuffled data within  $2\sigma$  for all redshifts.

The interpretation of the anisotropy within a framework of the FLRW model plus local boosts leads to a conundrum. The mismatch between the 350 km/s amplitude of a Local Group boost that would be consistent with the Hubble dipole anisotropy and the 635 km/s boost required to account for the CMB dipole kinematically suggests two possible solutions: (i) the galaxies in the COMPOSITE sample are in a coherent bulk flow with respect to the CMB on scales up to  $z \sim 0.045$ ; or (ii) the Hubble dipole and other anisotropies contain a substantial nonkinematic component.

While the bulk flow hypothesis is the one that is widely studied — being based on the standard FLRW model — it is at odds with the results of Wiltshire et al. (2013) that the spherically averaged, or monopole, Hubble expansion variation is very significantly reduced in the LG frame as compared to the CMB frame on  $\lesssim 70 h^{-1} \text{ Mpc}$  scales. The spherical average of a coherent bulk flow on such scales does not produce a monopole expansion variation of the character seen in the COMPOSITE sample (Wiltshire et al. 2013), and such a result is not seen in  $N$ -body Newtonian simulations<sup>4</sup>. Moreover, the signature of a systematic boost offset (3) from the LG to CMB frame is seen in both the COMPOSITE and Cosmicflows-2 samples (McKay & Wiltshire 2015), providing a potential explanation for the CMB frame monopole variation if the LG rest frame is closer to being the frame in which anisotropies in the Hubble expansion are minimized.

We will now investigate the extent to which a nonkinematic interpretation of the anisotropies is observationally consistent by ray tracing in exact inhomogeneous solutions of the Einstein equations.

#### 4. LIGHT PROPAGATION IN THE NON-LINEAR RELATIVISTIC REGIME AND THE ORIGIN OF ANISOTROPIES

Relativistic cosmological models predict the expansion of the Universe, which induces cosmological redshift. The expansion of space, however, does depend on the local coupling of matter and curvature, and only in the simplified spatially homogeneous and isotropic model is expansion uniform in space. The general relativistic formula for the redshift is (Ellis 1971)

$$\frac{1}{(1+z)^2} \frac{dz}{ds} = \frac{1}{3} \Theta + \Sigma_{ab} n^a n^b + u^a{}_{;b} u^b n_a, \quad (20)$$

where  $u^a$  is the matter velocity field,  $n_a$  is the connecting covector field locally orthogonal<sup>5</sup> to  $u^a$ ,  $\Sigma_{ab}$  is the

<sup>4</sup> The effect of a local boost of the central observer is the most significant aspect of our analysis. FLRW models with additional inhomogeneities produced by Newtonian  $N$ -body simulations do not lead to results significantly different from a pure FLRW model plus local boost shown as shown in Fig. 3. These results will be reported elsewhere (Bolejko et al. 2016).

<sup>5</sup> I.e.,  $u^a n_a = 0$ ,  $n_a n^a = 1$ . In the case that the vorticity of the velocity field vanishes — i.e.,  $u_{[a;b]} = 0$  — then  $n_a$  is also the normal to a spatial hypersurface with tangent  $u^a$ . For practical purposes, this is taken to be the case in cosmological averages.

shear of the velocity field, and  $\Theta = u^a_{;a}$  is its expansion. In the limit of spatially homogeneous and isotropic models the shear vanishes,  $\Sigma_{ab} \rightarrow 0$ , and the expansion of the velocity field reduces to the Hubble parameter,  $\Theta \rightarrow 3H(t)$ . However, once cosmic structures form, the expansion field becomes non-uniform (ranging from  $\Theta = 0$  inside virialized clusters of galaxies to  $\Theta > 3H_0$  within cosmic voids), and so the shear,  $\Sigma_{ab}$ , and acceleration,  $u^a_{;b}u^b$ , of the velocity field are nonzero.

Distances are also affected by presence of cosmic structures. The general relativistic framework that allows us to calculate the distance is based on the Sachs equations (Sachs 1961; Peebles 1993)

$$\frac{d^2 d_A}{ds^2} = - \left( \sigma^2 + \frac{1}{2} R_{ab} k^a k^b \right) d_A, \quad (21)$$

where  $k^a$  is the tangent to null geodesics in a congruence,  $\sigma = \frac{1}{2} \sigma_{ab} \sigma^{ab}$  is the scalar shear of the null geodesic bundle, and  $R_{ab}$  is the Ricci curvature. The luminosity distance  $d_L$  is then given by the reciprocity theorem (Etherington 1933; Ellis 1971)

$$d_L = (1 + z)^2 d_A. \quad (22)$$

Solving (21), (22) for the areal and luminosity distances, and (20) for the redshift, we arrive at a general relativistic distance–redshift relation, which will give rise to an anisotropic Hubble expansion generated by the spatial inhomogeneities in the geometric terms on the right hand sides of (20) and (21). The anisotropies will be most prominent over length scales characteristic of the matter inhomogeneities, and will have characteristics which are distinct from a simple FLRW geometry plus spatial boosts.

#### 4.1. The geometry and Einstein equations

In order to solve (20), (21) for the distance–redshift relation we need to calculate all relevant physical quantities such as the Ricci curvature, the shear of the null and timelike geodesic bundles, and the expansion scalar. For this purpose we use the Szekeres model (Szekeres 1975a), which is the most general known exact solution of the Einstein equations for an inhomogeneous dust source. In the limit of a spatially homogeneous matter distribution it reduces to the FLRW model.

The advantage of the Szekeres model over the FLRW model with linear perturbations is that we can account for relevant nonlinear effects associated with nonlinear inhomogeneities that are present in the local Universe. In particular, we will study a quasispherical Szekeres model generated by a spherical void onto which an additional inhomogeneity with an axial density gradient is superposed. Thus we have both overdense and underdense regions in the same exact solution of Einstein’s equations.

The Szekeres model reduces to the spherically symmetric LT model in the limit of no superposed axial density gradient. In the LT limit the anisotropy in the Hubble expansion is generated solely by the off–centre position of an observer relative to the centre of the inhomogeneity. In the Szekeres model this parameter will still play a role. However, the angle between the observer and the density gradient axis will also give rise to more complex and realistic anisotropies than are possible with the LT model alone. This allows us greater freedom to more closely

model actual structures in the local Universe. Of course, the Szekeres model still has limitations as to what it can describe. (We will return to this issue later on.)

The metric of the quasispherical Szekeres model (Szekeres 1975a,b) is usually represented in the following form

$$ds^2 = c^2 dt^2 - \frac{(R' - R \frac{\mathcal{E}'}{\mathcal{E}})^2}{1 - k} dr^2 - \frac{R^2}{\mathcal{E}^2} (dp^2 + dq^2), \quad (23)$$

where  $' \equiv \partial/\partial r$ ,  $R = R(t, r)$ , and  $k = k(r) \leq 1$  is an arbitrary function of  $r$ . The function  $\mathcal{E}$  is given by

$$\mathcal{E}(r, p, q) = \frac{1}{2S} (p^2 + q^2) - \frac{P}{S} p - \frac{Q}{S} q + \frac{P^2}{2S} + \frac{Q^2}{2S} + \frac{S}{2}, \quad (24)$$

where the functions  $S = S(r)$ ,  $P = P(r)$ ,  $Q = Q(r)$ , but are otherwise arbitrary. We take the coordinates  $r$ ,  $p$ ,  $q$  and the functions  $P$ ,  $Q$ ,  $R$ ,  $S$ ,  $\mathcal{E}$  all to have dimensions of length. We can also define angular coordinates,  $(\theta, \phi)$ , by

$$p - P = S \cot \frac{\theta}{2} \cos \phi, \quad q - Q = S \cot \frac{\theta}{2} \sin \phi. \quad (25)$$

Then  $\mathcal{E} = S/(1 - \cos \theta)$ , and the metric (23) takes the form

$$\begin{aligned} ds^2 = & c^2 dt^2 - \frac{1}{1 - k} \left[ R' + \frac{R}{S} (S' \cos \theta + N \sin \theta) \right]^2 dr^2 \\ & - \left[ \frac{S' \sin \theta + N (1 - \cos \theta)}{S} \right]^2 R^2 dr^2 \\ & - \left[ \frac{(\partial_\phi N) (1 - \cos \theta)}{S} \right]^2 R^2 dr^2 \\ & + \frac{2 [S' \sin \theta + N (1 - \cos \theta)]}{S} R^2 dr d\theta \\ & - \frac{2 (\partial_\phi N) \sin \theta (1 - \cos \theta)}{S} R^2 dr d\phi \\ & - R^2 (d\theta^2 + \sin^2 \theta d\phi^2), \end{aligned} \quad (26)$$

where  $N(r, \phi) \equiv (P' \cos \phi + Q' \sin \phi)$ .

The Einstein equations with cosmological constant,  $\Lambda$ , and dust source of mass density,  $\rho$ ,

$$G_{ab} - \Lambda g_{ab} = \kappa^2 \rho u_a u_b, \quad (27)$$

where  $\kappa^2 = 8\pi G/c^4$ , reduce to the evolution equation and the mass distribution equation. The evolution equation is

$$\dot{R}^2 = -k(r) + \frac{2M(r)}{R} + \frac{1}{3} \Lambda c^2 R^2, \quad (28)$$

where  $\dot{\phantom{x}} \equiv \partial/\partial t$ , and  $M(r)$  is a function related to the mass density by

$$\kappa \rho = \frac{2 (M' - 3M\mathcal{E}'/\mathcal{E})}{R^2 (R' - R\mathcal{E}'/\mathcal{E})}. \quad (29)$$

Note that

$$\frac{\mathcal{E}'}{\mathcal{E}} = \frac{-1}{S} [S' \cos \theta + N \sin \theta] \quad (30)$$

is the only term in (29) which gives a departure from spherical symmetry. One is free to specify the various



functions as long as (28)–(30) are satisfied. Since  $R(t, r)$  is the only function that depends on time, (28) can be integrated to give

$$t - t_B(r) = \int_0^R \frac{d\tilde{R}}{\sqrt{-k + 2M/\tilde{R} + \frac{1}{3}\Lambda c^2 \tilde{R}^2}}, \quad (31)$$

where  $t_B(r)$  is one more arbitrary function called the *bang time* function, which describes the fact that the age of the Universe can be position dependent. If we demand that the age of the Universe is everywhere the same for comoving observers — the homogeneous Big Bang condition — then the above equations link  $M(r)$  and  $k(r)$ . In the generic case  $M$  and  $k$  can be arbitrary, which could mean either a non-uniform Big Bang, or some turbulent initial conditions; i.e., conditions that would require a more complicated model than the Szekeres model.

The matter distribution in the Szekeres model has a structure of a dipole superposed on a monopole, (cf., upper left panel of Fig. 4). In order to determine the Szekeres model and solve all the equations, we need to specify its five arbitrary functions. These are:  $M$  and  $k$  which describe the monopole distribution, and  $S$ ,  $P$ , and  $Q$  which describe the dipole. If  $S$ ,  $P$ ,  $Q$  are constant the dipole vanishes and we recover spherical symmetry; if  $S' \neq 0$ , and  $P' = 0 = Q'$  then the model is axially symmetric. These five functions (or any other combination of functions from which these can be evaluated) are sufficient to solve all the equations that describe the evolution of matter and light propagation in the evolving geometry.

In the FLRW limit when the model becomes spatially homogeneous and isotropic we have:

$$R \rightarrow ra(t) \quad (32)$$

$$M \rightarrow M_0 r^3, \quad (33)$$

$$k \rightarrow k_0 r^2, \quad (34)$$

where  $M_0 = \frac{1}{2}H_0^2\Omega_m$ ,  $k_0 = H_0^2(\Omega_m + \Omega_\Lambda - 1)$ , and the functions  $S$ ,  $P$ , and  $Q$  are constant ( $S' = 0 = P' = Q'$ ). Therefore, in the FLRW limit the dependence on  $r$  in (28) cancels out and after dividing by  $a^2$  we recover the well known form of the Friedmann equation

$$H^2 = H_0^2 (\Omega_m a^{-3} + \Omega_k a^{-2} + \Omega_\Lambda),$$

where  $\Omega_\Lambda = \Lambda c^2/(3H_0^2)$ , and  $\Omega_m + \Omega_k + \Omega_\Lambda = 1$ .

Let us then model the departure from homogeneity using the following profile of the mass function

$$M = M_0 r^3 [1 + \delta_M(r)], \quad (35)$$

where

$$\delta_M(r) = \frac{1}{2}\delta_0 \left(1 - \tanh \frac{r - r_0}{2\Delta r}\right), \quad (36)$$

with  $-1 \leq \delta_0 < 0$ , is a localized perturbation which is underdense at the origin. As  $r \rightarrow \infty$ , we have  $\delta_M \rightarrow 0$  so that the spatial geometry is asymptotically that of the homogeneous and isotropic FLRW model. We normalize this geometry by choosing the spatially flat  $\Lambda$ CDM model which best fits the Planck satellite data, with  $\Omega_m = 0.315$  and  $H_0 = 67.3 \text{ km s}^{-1} \text{ Mpc}^{-1}$  (Ade et al. 2014a).

The function  $k(r)$  is then evaluated from (31) for each  $r$  under the assumptions: (i) the age of the Universe is everywhere the same for comoving observers,  $t_B = 0$ ; and (ii)  $R(t_0, r) = r$  for each  $r$ , where the age of the Universe,  $t_0$ , is equal to that of the asymptotic background spatially flat FLRW model.

Finally we assume axial symmetry, with dipole described by only the function  $S$ , which we choose to be:

$$\begin{aligned} S &= r \left( \frac{r}{1 \text{ Mpc}} \right)^{\alpha-1}, \\ P &= 0, \\ Q &= 0, \end{aligned} \quad (37)$$

where  $\alpha$  is a free parameter. When  $\alpha \rightarrow 0$  the model becomes the spherically symmetric LT model, as shown in the lower left panel of Fig. 4.

The model has 7 free parameters:

- 4 parameters that specify the Szekeres model  $\alpha$ ,  $\delta_0$ ,  $r_0$ ,  $\Delta r$ ,
- 3 parameters that specify the position of the observer  $r_{obs}$ ,  $\varphi_{obs}$ ,  $\vartheta_{obs}$ .

Since the model considered here is axially symmetric, we can choose the observer to lie in the plane  $\varphi_{obs} = \pi/2$  without loss of generality. In order to reduce the dimension of the parameter space we also set  $\Delta r = 0.1r_0$  for simplicity. That leaves us with 5 parameters. In reality, we expect the perturbations that describe actual cosmic structures to be much more complicated than the parameterization adopted here. So while this gives us some flexibility, not all structures can be described using this parameterization. The structures that can be described using this parameterization consist of a void and an adjacent overdensity, as presented in the upper left panel of Fig. 4. While not perfect, this parameterization aims to model some of the major structures in the local Universe, such as the Local Void and the overdensity known as the Great Attractor (Tully et al. 2008).

By varying the five free parameters, we can tune the size of the void and/or overdensity, the amplitude of the density contrast and the position of the observer relative to the structures. We run a search through this 5-dimensional parameter space looking for a model which as closely as possible satisfies constraints in the following order of importance:

1. The CMB temperature has a maximum value of  $T_0 + \Delta T$  relative to the mean  $T_0 = 2.725 \text{ K}$ , where  $\Delta T(\ell = 276.4^\circ, b = 29.3^\circ) = 5.77 \pm 0.36 \text{ mK}$ , which corresponds to the CMB temperature dipole amplitude and direction in the LG rest frame.
2. The quadrupole of the CMB anisotropy is lower than the observed value (*Planck Legacy Archive* 2013)

$$C_{2,CMB} < 242.2^{+563.6}_{-140.1} \mu\text{K}^2.$$

While the dipole of the CMB is significantly affected by local expansion, the quadrupole is dominated by the physics of the early universe, and

the observed value itself is about 5 times smaller than the standard  $\Lambda$ CDM expectation. Therefore we implement this constraint to ensure that the quadrupole generated by local inhomogeneities is much lower than the quadrupole generated at last scattering.

3. The dipole of the Hubble expansion anisotropy and its redshift dependence must be consistent with the observed anisotropy of the COMPOSITE sample as presented in Fig. 3.
4. The quadrupole of the Hubble expansion anisotropy and its redshift dependence must be consistent with the observed anisotropy of the COMPOSITE sample as presented in Fig. 3.

#### 4.2. Constructing mock catalogues

The algorithm of our analysis can be summarized by the following steps:

1. We first specify the Szekeres model.
2. We apply the HEALPix grid of the sky and propagate light rays in these directions.
3. We then calculate the CMB temperature maps.
4. We use HEALPix routines to calculate the anisotropy of the CMB map.
5. We take the COMPOSITE sample. For each galaxy we have its angular position  $(\ell_i, b_i)$ , luminosity distance  $d_i$ , uncertainty in distance  $\Delta d_i$  and redshift  $z_i$ . For each of these directions  $(\ell_i, b_i)$  we numerically propagate light rays, using the null geodesic equations of the Szekeres model, up until  $d = d_i$ . We then write down the redshift evaluated within the Szekeres model  $z_{Sz}$ .
6. We construct the mock COMPOSITE catalogue, by replacing  $z_i$  with  $z_{Sz}$ , (i.e., the redshift obtained in the Szekeres model for this direction and this distance).
7. We construct 100,000 mock catalogues, by taking into account uncertainty in the distance. This is done by replacing the distance from the COMPOSITE sample with the distance  $d_N$

$$d_N = \mathcal{N}(\mu = d_i, \sigma = \Delta d_i).$$

which equal to a random number drawn from a Gaussian distribution whose mean value is  $d_i$  and standard deviation equal to distance uncertainty.

8. For each of these mock catalogues we calculate the Hubble expansion and its anisotropy as outlined in Sec. 3.1.

#### 4.3. Anisotropy of the Hubble expansion generated by cosmic structures modelled by the Szekeres model

Our search through the 5-dimensional parameter leads us to a model, whose mass profile as well as the position

of the observer are presented in the upper left panel of Fig. 4. The values of the free parameters are

$$\begin{aligned} \alpha &= 0.86, \\ \delta_0 &= -0.86, \\ r_0 &= 38.5 \, h^{-1} \text{ Mpc}, \\ \Delta r &= 3.85 \, h^{-1} \text{ Mpc}, \end{aligned} \quad (38)$$

and the position of the observer:

$$\begin{aligned} r_{obs} &= 25 \, h^{-1} \text{ Mpc}, \\ \varphi_{obs} &= 0.5\pi, \\ \vartheta_{obs} &= 0.705\pi. \end{aligned} \quad (39)$$

These distances are coordinate distances, not radial proper distances or luminosity distances.

Interestingly, if take the region of maximum overdensity in Fig. 4, with density contrast  $\delta\rho/\rho > 2$ , this region is found to be located at redshifts and luminosity distances in the ranges  $0.003 \lesssim z \lesssim 0.013$  and  $16 \, h^{-1} \lesssim D_L \lesssim 53 \, h^{-1} \text{ Mpc}$ , comparable to those of the Centaurus cluster / Great Attractor<sup>6</sup>. We did not supply the redshift of the overdensity as an *a priori* constraint, but arrived at it using a grid search on possible Szekeres models following the criteria specified above.

The anisotropy of the Hubble expansion within such a model is presented in the upper panels of Fig. 4. We find that the first three criteria given in Sec. 4.2 are all satisfied. In particular, the CMB temperature dipole is

$$T_{CMB} = 5.58 \text{ mK},$$

as is expected in the LG frame, while the quadrupole of the CMB temperature anisotropy is

$$C_{2,CMB} = 8.26 \, \mu\text{K}^2.$$

Furthermore, the dipole of the Hubble expansion within this model is consistent with the dipole of the Hubble expansion inferred from the COMPOSITE sample.

The results shown in Fig. 4 display the clear advantage of the Szekeres model in comparison with a FLRW model plus local boosts, as discussed in Sec. 3.3. Applying a local boost to an otherwise homogeneous and isotropic universe we found that it was not possible to fit the Hubble expansion dipole and the CMB temperature dipole simultaneously. By contrast the Szekeres model simultaneously matches both the CMB temperature dipole in the LG frame and the Hubble expansion dipole of the COMPOSITE sample over all redshifts in the survey with sufficient data. Given the fact that the structure of the Universe on scales below  $100 \, h^{-1} \text{ Mpc}$  is very inhomogeneous, and that differential expansion of space is a generic feature of cosmological solutions of Einstein's equation, it should perhaps not be a surprise that the inhomogeneous model performs better.

On the other hand, the particular Szekeres model considered here is not able to reproduce the quadrupole of the Hubble expansion seen in the COMPOSITE sample, which is about three times larger in magnitude than in the simulation. The Hubble expansion quadrupole in the

<sup>6</sup> The Centaurus cluster, at LG frame redshift of  $z = 0.0104 \pm 0.0006$  (Struble & Rood 1999), lies in the nearer portion of the Great Attractor region (Courtois et al. 2013).

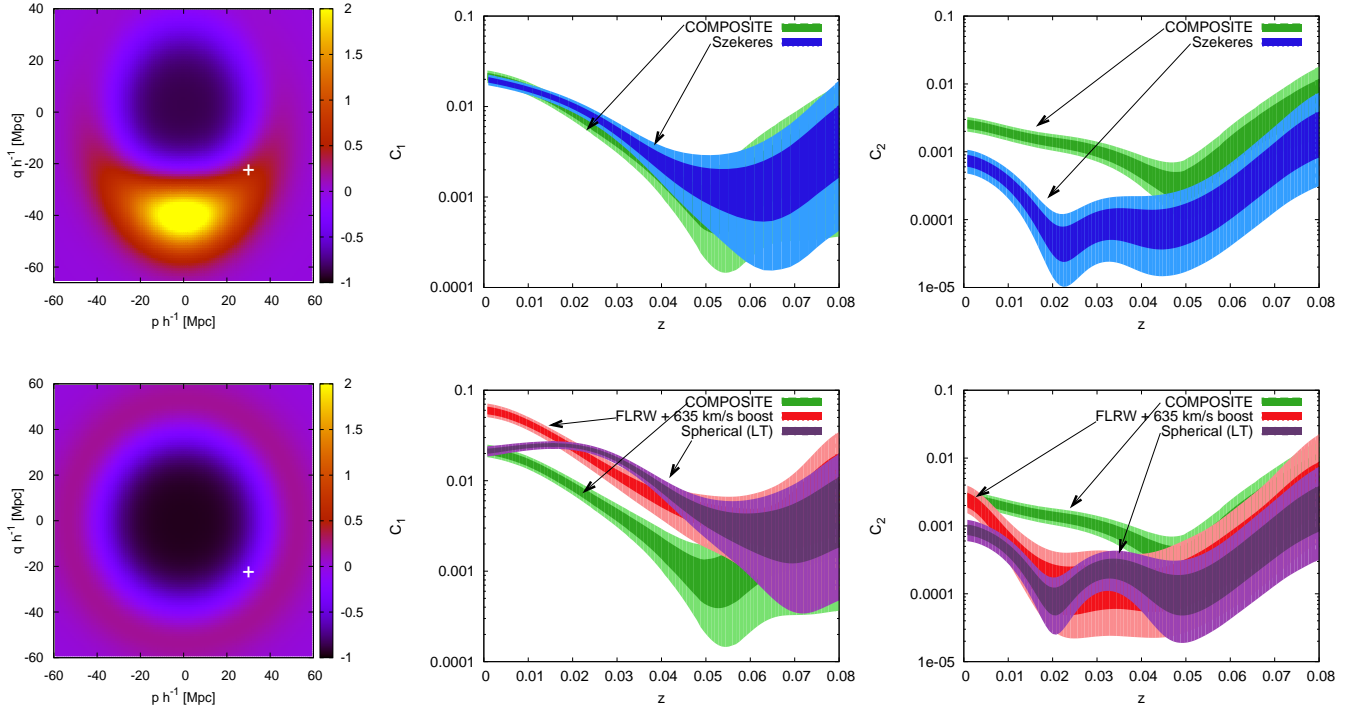


**Figure 4.** The anisotropy of the Hubble expansion. *Upper Panels* show the anisotropy of the Hubble expansion within the Szekeres model, whose density distribution is presented in the upper left panel (this panel shows the density contrast,  $\delta_\rho = (\rho - \bar{\rho})/\bar{\rho}$  given in the right hand scale, when smoothed with Gaussian kernel of size  $8 h^{-1} \text{Mpc}$ ); the position of the observer is marked with a cross “+”. *Lower Panels* show the anisotropy of the Hubble expansion within the spherical model (LT) model, whose density distribution is presented in the lower left panel (cross “+” marks the position of the observer); the anisotropy of the Hubble expansion evaluated within the FLRW model with a local boost of 635 km/s is also presented for comparison.

Szekeres model (35)–(39) in fact has an amplitude consistent with that of the randomly reshuffled data in Fig. 2, and is not statistically significant.

The fact that we can account for the Hubble expansion dipole, but not the quadrupole may well be due to the simplicity of the model (35)–(39), (cf., upper panel of Fig. 4). In particular, the choice (37) enforces an axial symmetry on the mass distribution, which could be altered to give finer details. This would require a more complex model, and is left for future investigations.

As an indication of how the properties of the Hubble expansion variation are induced by changes in the matter distribution, we have also investigated the anisotropy of the Hubble expansion evaluated using a spherical void LT model, which is obtained from the Szekeres model in the limit of a vanishing matter dipole,  $\alpha \rightarrow 0$ .

We use the same parameterization and procedure as outline above with  $\alpha = 0$ , which ensures spherical symmetry. As in the case of a simple boost (Sec. 3.3) we are not able to simultaneously fit the CMB temperature variation and the full redshift dependence of the Hubble expansion anisotropy. At best, we can only reproduce some of the features.

An example of this investigation is presented in lower panels of Fig. 4. The values of the free parameters are

$$\begin{aligned} \alpha &= 0, \\ \delta_0 &= -0.95, \end{aligned}$$

$$\begin{aligned} r_0 &= 45.5 h^{-1} \text{Mpc}, \\ \Delta r &= 4.55 h^{-1} \text{Mpc} \end{aligned}$$

and the position of the observer is

$$\begin{aligned} r_{obs} &= 28 h^{-1} \text{Mpc}, \\ \varphi_{obs} &= 0.5\pi, \\ \vartheta_{obs} &= 0.5\pi. \end{aligned}$$

(40)

The model matches the correct temperature dipole of the CMB in the LG frame

$$\Delta T_{\text{CMB}} = 5.63 \text{ mK}$$

and the quadrupole of the CMB temperature anisotropy is

$$C_{2,\text{CMB}} = 20.73 \mu\text{K}^2.$$

However, the Hubble expansion dipole anisotropy can only be matched at very low redshifts (see middle panel of Fig. 4). As the redshift is increased the magnitude of the dipole increases until for,  $z > 0.015$ , it becomes consistent with that predicted by the FLRW model plus a local boost of 635 km/s in the LG frame — which was not consistent with the COMPOSITE data, however.

This illustrates the fact that the amplitudes of the CMB dipole and higher multipoles in LT models can be roughly estimated for off-centre observers by an effective Newtonian approximation Alnes & Amarzguioui

(2006) using the velocity appropriate to a boosted observer in the FLRW geometry. This limit was discussed by Wiltshire et al. (2013), who gave an example of a LT void with a somewhat different mass profile but with similar parameters, being 18% larger but with a less sharp density gradient.

An examination of the density profile panels of Fig. 4 illustrates the role that is played by differential expansion of space. In particular, Lorentz boosts represent a point symmetry in the tangent space of any general observer. In the case of the LT model, the axis which joins the centre of the void to the position of the off-centre observer defines a direction along which a radial boost can be taken to act from the void centre. Since the differential expansion is purely radial with respect to the centre, it still somewhat mimics the action of a point symmetry. Thus it is not surprising that the LT dipole becomes equivalent to the FLRW model plus boost on scales larger than  $r_0 + r_{obs}$ . By contrast, the Szekeres model incorporates a mass dipole on an axis distinct from that joining  $r_0$  to  $r_{obs}$ . This distributed density gradient therefore gives rise to a differential expansion of space which cannot be mimicked by a boost or any other point symmetry relative to the central point,  $r_0$ .

The models considered in this Section show how the presence of cosmic structures affect the anisotropy of the Hubble expansion. The more structures that are present in the model, the better is the consistency with observational data.

## 5. POTENTIAL IMPACT ON CMB ANOMALIES

We have seen that an exact inhomogeneous Szekeres model which is equivalent to the standard Planck-satellite normalized  $\Lambda$ CDM model on  $\gtrsim 100 h^{-1}\text{Mpc}$  scales but which exhibits differential expansion of space on  $\lesssim 100 h^{-1}\text{Mpc}$  scales relative to the LG frame is able to consistently fit more features of the Hubble expansion anisotropy seen in the COMPOSITE sample on  $\lesssim 100 h^{-1}\text{Mpc}$  scales, as compared to the case in which the Local Group of galaxies is boosted relative to a FLRW model at rest in the CMB frame.

If this is further supported by more detailed models with additional structures, then it potentially has major implications for large angle anomalies in the CMB (Ade et al. 2014b), as has been discussed by Wiltshire et al. (2013), since it is conventionally assumed that the CMB dipole is entirely kinematic.

This means that the differential expansion of space due to relatively local structures can affect the redshift of the CMB photons, thereby affecting the CMB temperature. This raises the possibility that part of the CMB temperature dipole could be of nonkinematic origin. While the Planck team (Aghanim et al. 2014) claim to have directly measured the kinematic nature of the CMB dipole through the effects of modulation and aberration on the CMB anisotropy spectrum, their result depends on the angular scale. In particular, the results of Aghanim et al. (2014) agree with the conventional boost direction,  $(\ell, b) = (264^\circ, 48^\circ)$  only if small angle multipoles are included in the analysis, with a definitive measurement for multipoles in the range  $l_{\min} = 500 < l < l_{\max} = 2000$ . If large angle multipoles are included and  $l_{\max}$  is reduced to  $l_{\max} < 100$ , then the inferred boost

direction moves across the sky to coincide with the modulation dipole anomaly direction (Hoftuft et al. 2009),  $(\ell, b) = (224^\circ, -22^\circ) \pm 24^\circ$ .

It is this angular scale dependence of the standard kinematic analysis (Aghanim et al. 2014), and its association with the angular anomaly directions on large scales, which is a hint that the hypothesis of Wiltshire et al. (2013) may be correct. The inhomogeneities in question are relatively nearby voids and overdensities, which subtend large angles on the sky. Furthermore, by the hypothesis of Wiltshire et al. (2013) part of the CMB dipole (due to the motion of the Sun and Milky Way within the LG) is still kinematic. When adding a kinematic and nonkinematic dipole the result may still look kinematic on angular scales much smaller than the scales subtended by the relevant structures on the sky. For example, a kinematic Newtonian approximation to the anisotropy seen by an off-centre in a LT void provides an accurate estimate of the magnitude of the CMB dipole but overestimates the magnitude of the CMB quadrupole to dipole ratio,  $C_2/C_1$ , of the LT model by a factor close to 2 (Alnes & Amarzguioui 2006; Wiltshire et al. 2013).

In practice, a kinematic dipole is subtracted from the CMB anisotropy data before the removal of galactic foregrounds. Therefore it is a complex task to practically test the hypothesis that large angle anomalies are a consequence of incorrectly treating the differential expansion of space in the local universe. We need to

- Refine the Szekeres model by the addition of structures to replicate the Hubble expansion quadrupole of the magnitude seen in the COMPOSITE sample;
- Confirm the Hubble expansion anisotropies seen in the COMPOSITE sample with other data sets. In the case of the Cosmicflows-2 sample (Tully et al. 2013), for example, this requires a careful treatment of Malmquist biases to remove a monopole bias (Hoffman et al. 2015; McKay & Wiltshire 2015);
- Once an accurate Szekeres model is obtained, confirmed by observational data sets, then such models need to be applied as an alternative to a Lorentz boost at appropriate stages of the pipeline in cleaning the CMB anisotropy maps to remove galactic foregrounds.

These steps involve many complications. However, the analysis to date is consistent with such a procedure having a positive outcome. In particular, if we introduce additional structures to produce a larger Hubble expansion quadrupole, then we might expect it to also produce a larger CMB temperature quadrupole. Since the CMB quadrupole for the Szekeres model of Sec. 4.3 is 30 times smaller in amplitude than the observed CMB quadrupole, we should reasonably expect that this can be accommodated.

## 6. CONCLUSION

Cosmic structures such as voids, sheets, filaments, and knots participate differently in the expansion of the Universe. The expansion rate gradually changes from no expansion inside virialized high density regions such as

superclusters to a higher than average expansion rate inside voids. This differential expansion of the space can be observed in the anisotropy of the Hubble expansion, especially on scales up to a few hundreds megaparsecs. In general relativity, differential expansion of space is the norm in all cosmological models which are not spatially homogeneous and isotropic. The anisotropy of the Hubble expansion is thus expected to quantitatively differ from that of a FLRW model in which all departures from homogeneity can be described by local Lorentz boosts of the source and observer.

In this paper we investigated the anisotropy pattern of the Hubble expansion, considering the monopole, dipole and quadrupole variations in the LG frame. Most previous studies have either focused on the monopole, i.e., the global (average) value of  $H_0$ , or on bulk flows, related to the volume average of peculiar velocities in the CMB frame, using methods which presuppose the validity of the perturbed FLRW framework, with nonlinear effects computed purely by Newtonian  $N$ -body simulations.

In a way this is analogous to studies of the CMB in 1970s–1990s. However, with increasing amount of data and precision of measurements, we are slowly arriving at the stage where we can study anisotropies of the Hubble expansion, just as we now study the anisotropy of the CMB temperature fluctuations.

In analogy to CMB temperature fluctuations, we show that the Hubble expansion can be decomposed using spherical harmonics and expressed in terms of an angular power spectrum. Moreover, by averaging data at various redshifts we can have additional information about the redshift dependence of the multipoles of the Hubble expansion. Irrespective of any theoretical assumptions about cosmic expansion, this is a novel technique that carries complimentary if not additional information to studies of bulk flow that have been extensively carried out in the past years.

In Sec. 3.1 we developed the formalism used to study the anisotropy of the Hubble expansion. When applied to the COMPOSITE sample we identified the presence of dipole and quadrupole anisotropies in the Hubble expansion. These anisotropies are statistically significant in the data up to  $z \lesssim 0.045$ . For larger redshifts the amount of data is small and the signal is no longer distinguishable from noise.

We compared the measured anisotropy with predictions from a FLRW model assumed to be homogeneous and isotropic in the CMB frame, and also particular LT and Szekeres models with small scale inhomogeneities in the LG frame. All models were assumed to be identical to a spatially flat FLRW models on scales  $\gtrsim 100 h^{-1}\text{Mpc}$ , with parameters fixed to those of the  $\Lambda\text{CDM}$  model that best fits the Planck satellite data (Ade et al. 2014a). The FLRW model with a local boost from the CMB to LG frame did not fit the observed redshift dependence of the dipole of the Hubble expansion of the COMPOSITE sample as seen in the LG frame. In order to match the observed features of the dipole of the Hubble expansion, the local boost would have to be reduced to approximately 350 km/s, which is much smaller than the actual  $635 \pm 38$  km/s that is required if the CMB temperature dipole is purely kinematic.

A quasispherical Szekeres solution that allows for vari-

ations of the local geometry generated by the presence of cosmic structures, which effectively model the Local Void and “Great Attractor”, was found to improve the fit. This analysis shows that the local cosmological environment does affect the Hubble expansion. Physically, this can be understood in terms of the differential expansion of the space, with the void expanding faster and the overdensity expanding at a slower than the average expansion rate.

As yet, the numerical model does not have a Hubble quadrupole as large as that seen in the COMPOSITE sample. However, if extra modifications are added — for example, by using methods to include extra structures (Sussman & Gaspar 2015b) — then given the magnitude of the effects that remain to be explained, it is highly plausible that highly accurate models of the local cosmic expansion can be developed. This is left for future work. As discussed in Sec. 5, this may potentially provide a simple physical explanation of particular large anomalies in the CMB radiation, in terms of known physics. Differential expansion of space is a natural feature of dust solutions of the Einstein equations, but it is not included in the standard model of cosmology. It is high time that this possibility is considered seriously, given the far reaching consequences this would have.

*Acknowledgements* This work was supported by the Marsden Fund of the Royal Society of New Zealand, and by the Australian Research Council through the Future Fellowship FT140101270. Computational resources used in this work were provided by Intersect Australia Ltd and the University of Sydney Faculty of Science.

## REFERENCES

- Ade, P. A. R., Aghanim, N., Armitage-Caplan, C., et al. 2014a, *A&A*, **571**, A16
- Ade, P. A. R., Aghanim, N., Armitage-Caplan, C., et al. 2014b, *A&A*, **571**, A23
- Aghanim, N., Armitage-Caplan, C., Arnaud, M., et al. 2014, *A&A*, **571**, A27
- Alnes, H., & Amarzguoui, M. 2006, *PhRvD*, **74**, 103520
- Amanullah, R., Lidman, C., Rubin, D., et al. 2010 *ApJ*, **716**, 712.
- Arnau, J. V., Fullana, M. J., Monreal, L., & Sáez, D. 1993, *ApJ*, **402**, 359
- Arnau, J. V., Fullana, M. J., & Sáez, D. 1994, *MNRAS*, **268**, L17
- Bacon, D. J., Andrianomena, S., Clarkson, C., Bolejko, K. & Maartens, R. 2014, *MNRAS*, **443**, 1900
- Bilicki, M., Peacock, J. A., Jarrett, T. H., Cluver, M. E., & Steward, L. 2014, *arXiv:1408.0799*
- Bolejko, K. 2006, *PhRvD*, **73**, 123508
- Bolejko, K. 2005, *PhRvD*, **75**, 043508
- Bolejko, K. & Hellaby, C. 2008, *GReGr*, **40**, 1771
- Bolejko, K. 2009, *GReGr*, **41**, 1737
- Bolejko, K., & Célérier, M. N. 2010, *PhRvD*, **82**, 103510
- Bolejko, K., & Sussman, R. A. 2011, *PhLB*, **697** 265
- Bolejko, K., Clarkson, C., Maartens, R., Bacon, D., Meures, N. & Beynon, E. 2013, *PhRvL*, **110**, 021302
- Bolejko, K., et al. 2016, in preparation
- Bondi, H. 1947, *MNRAS*, **107**, 410
- Buckley, R. G. & Schlegel, E. M. 2013, *PhRvD*, **87**, 023524
- Clowes, R. G., Harris, K. A., Raghunathan, S., Campusano, L. E., Soechting, I. K., & Graham, M. J. 2013, *MNRAS*, **429**, 2910
- Copi, C. J., Huterer, D., Schwarz, D. J., & Starkman, G. D. 2006, *MNRAS*, **367**, 79
- Courtois, H. M., Pomarède, D., Tully, R. B., Hoffman, Y., Courtois, D. 2013, *AJ*, **146**, 69
- de Oliveira-Costa, A., Tegmark, M., Zaldarriaga, M., & Hamilton, A. 2004, *PhRvD*, **69**, 063516

- Duley, J. A. G., Nazer, M. A., & Wiltshire, D. L. 2013, CQGra, **30**, 175006
- Einasto, J. 2014, arXiv:1410.6932
- Ellis, G. F. R. 1971, in *Proceedings of the International School of Physics 'Enrico Fermi', Course 47: General Relativity and Cosmology*, ed. R. K. Sachs (Academic Press, New York and London), pp. 104–182; reprinted, with historical comments, in 2009, GReGr, **41** 581.
- Erdoğdu, P., Lahav, O., Huchra, J. P., et al. 2006, MNRAS, **373**, 45
- Eriksen, H. K., Hansen, F. K., Banday, A. J., Górski, K. M., & Lilje, P. B. 2004, ApJ, **605**, 14; (E) **609**, 1198
- Eriksen, H. K., Banday, A. J., Górski, K. M., Hansen, F. K., & Lilje, P. B. 2007, ApJ, **660**, L81
- Etherington, I. M. H. 1933, Phil. Mag. VII, 15, 761; reprinted, with historical comments, in 2007, GReGr, **39**, 1055.
- Feldman, H. A., Watkins, R., & Hudson, M. J. 2010, MNRAS, **407**, 2328
- Forero-Romero, J. E., Hoffman, Y., Gottlöber, S., Klypin, A., & Yepes, G. 2009, MNRAS, **396**, 1815
- Górski, K. M., Hivon, E., Banday, A. J., Wandelt, B. D., Hansen, F. K., Reinecke, M. & Bartelman, M., 2005, ApJ, **622**, 759
- Hicken M., Wood-Vasey W. M., Blondin S., Challis P., Jha S., Kelly P. L., Rest A., & Kirshner R. P. 2009, ApJ, **700**, 1097.
- Hoffman, Y., Courtois, H. M., & Tully, R. B. 2015, arXiv:1503.05422.
- Hoftuft, J., Eriksen, H. K., Banday, A. J., Górski, K. M., Hansen, F. K., & Lilje, P. B. 2009, ApJ, **699**, 985
- Hogg, D. W., Eisenstein, D. J., Blanton, M. R., Bahcall, N. A., Brinkmann, J., Gunn, J. E., & Schneider, D. P. 2005, ApJ, **624**, 54
- Hoyle, F., & Vogeley, M. S. 2002, ApJ, **566**, 641
- Hoyle, F., & Vogeley, M. S. 2004, ApJ, **607**, 751
- Humphreys, N. P., Maartens, R., & Matraers, D. R. 1997, ApJ, **477**, 47
- Ishak, M., & Peel, A. 2012, PhRvD, **85**, 083502 [arXiv:1104.2590]
- Kim, J., & Naselsky, P. 2010, ApJ, **714**, L265
- Kowalski, M., et al. 2008, ApJ, **686**, 749
- Land, K., & Magueijo, J. 2005, PhRvL, **95**, 071301
- Lemaître, G. 1933, Ann. Soc. Sci. Bruxelles A, **53**, 51 [English translation: 1997, GReGr, **29**, 641]
- Li, N., & Schwarz, D. J. 2008, PhRvD, **78**, 083531
- McClure, M. L., & Dyer, C. C. 2007, NewA, **12**, 533
- McKay, J. H., & Wiltshire, D. L. 2015, arXiv:1503.04192
- Nwankwo, A., Ishak, M., & Thompson, J. (2011), JCAP 05(2011), 028
- Pan, D. C., Vogeley, M. S., Hoyle, F., Choi, Y. Y., & Park, C. 2012, MNRAS, **421**, 926
- Partridge, R. B., & Wilkinson, D. T. 1967, PhRvL, **18**, 557
- Peebles, P. J. E., *Principles of Physical Cosmology*, Princeton University Press (1993).
- Peebles, P. J. E., & Wilkinson, D. T. 1968, PhRv, **174**, 2168
- Planck Legacy Archive* 2013, COM\_PowerSpect-CMB\_R2.01.fits, <http://www.cosmos.esa.int/web/planck/pla>
- Riess, A. G., Macri, L., Casertano, S., et al. ApJ, **730**, 119; (E) **732**, 129
- Roukema, B. F., Buchert, T., Ostrowski, J. J., & France, M. J. 2015, MNRAS, **448**, 1660
- Sachs, R. 1961, RSPSA, **264**, 309
- Schwarz, D. J., Starkman, G. D., Huterer, D., & Copi, C. J. 2004, PhRvL, **93**, 221301
- Scrimgeour, M., Davis, T., Blake, C., et al. 2012, MNRAS, **425**, 116
- Stewart, J. M., & Sciamia, D. W. 1967, Nature **216**, 748
- Struble, M. F., & Rood, H. J. 1999, ApJS **125**, 35
- Sussman, R. A. & Gaspar I. D. 2015, arXiv:1507.02306
- Sussman, R. A. & Gaspar I. D. 2015, PhRvD, **92**, 083533.
- Sylos Labini, F., Vasilyev, N. L., Pietronero, L., & Baryshev, Y. V. 2009, Europhys. Lett. **86**, 49001
- Szekeres, P. 1975a, Commun. Math. Phys. **41**, 55
- Szekeres, P. 1975b, PhRvD, **12**, 2941
- Tegmark, M., de Oliveira-Costa, A., & Hamilton, A. J. S. 2003, PhRvD, **68**, 123523
- Tikhonov, A. V., & Karachentsev, I. D. 2006, ApJ, **653**, 969 .
- Tolman, R. C. 1934, Proc. Nat. Acad. Sci. **20**, 169
- Tomita, K. 2000, ApJ, **529**, 26.
- Tully B. R., Shaya J. E., Karachentsev D. I., Courtois M. H., Kocevski D. D., Rizzi L., & Peel A. 2008, ApJ, **676**, 184.
- Tully R. B., Courtois H. M., Dolphin A. E., et al. 2013, AJ, **146**, 86.
- Watkins, R., Feldman, H. A., & Hudson, M. J. 2009, MNRAS, **392**, 743
- Wiltshire, D. L. 2007a, New J. Phys. 9, 377
- Wiltshire, D. L. 2007b, PhRvL, **99**, 251101
- Wiltshire, D. L. 2009, PhRvD, **80**, 123512
- Wiltshire, D. L., Smale, P. R., Mattsson, T., & Watkins, R. 2013, PhRvD, **88**, 083529 .